Efficient 18.8 T MAS-DNP NMR reveals hidden side chains in amyloid fibrils

Alons Lends, Nicolas Birlirakis, Xinyi Cai, Asen Daskalov, Jayakrishna Shenoy, Muhammed Bilal Abdul-Shukkoor, Mélanie Berbon, Fabien Ferrage, Yangping Liu, Antoine Loquet, et al.

Efficient 18.8 T MAS-DNP NMR reveals hidden side chains in amyloid fibrils

Alons Lends[1], Nicolas Birlirakis[2], Xinyi Cai[3], Asen Daskalov[1], Jayakrishna Shenoy[1], Muhammed Bilal Abdul-Shukkoor[1], Mélanie Berbon[1], Fabien Ferrage[2], Yangping Liu[3], Antoine Loquet[1*], Kong Ooi Tan[2*]

[1]CNRS, Chemistry and Biology of Membranes and Nanoobjects (CBMN), UMR 5348, Institut Europeen de Chimie et Biologie (IECB), University of Bordeaux, F-33600, Pessac, France.

[2]Laboratoire des Biomolécules, LBM, Département de Chimie, École Normale Supérieure, PSL University, Sorbonne Université, CNRS, 75005 Paris, France.

[3]Tianjin Key Laboratory on Technologies Enabling Development of Clinical Therapeutics and
Diagnostics, School of Pharmacy, Tianjin Medical University, Tianjin 300070, China.

Corresponding Authors:
Kong Ooi Tan (kong-ooi.tan@ens.psl.eu)
Antoine Loquet (a.loquet@iecb.u-bordeaux.fr)

Keywords: Amyloid Fibrils, Solid-State NMR, Dynamic Nuclear Polarization

Abstract

Amyloid fibrils are large and insoluble protein assemblies composed of a rigid core associated with a cross-β arrangement rich in β-sheet structural elements. It has been widely observed in solid-state NMR experiments that semi-rigid protein segments or side chains do not yield easily observable NMR signals at room temperature. The reasons for the missing peaks may be due to the presence of unfavorable dynamics that interfere with NMR experiments, which result in very weak or unobservable NMR signals. Therefore, for amyloid fibrils, semi-rigid and dynamically disordered segments flanking the amyloid core are very challenging to study. Here, we show that high-field dynamic nuclear polarization (DNP), an NMR hyperpolarization technique typically performed at low temperatures, can circumvent this issue because (i) the low-temperature environment (~ 100 K) slows down the protein dynamics to escape unfavorable detection regime, (ii) DNP improves the overall NMR sensitivity including flexible side chains, and (iii) efficient cross-effect DNP biradicals (SNAPol-1) optimized for high-field DNP (≥ 18.8 T) are employed to offer high sensitivity and resolution suitable for biomolecular NMR applications. By combining these factors, we have successfully recorded an unprecedented enhancement factor of ε~50 on amyloid fibrils using an 18.8 T/ 800 MHz magnet. We have compared the DNP efficiencies of M-TinyPol, NATriPol-3, and SNAPol-1 biradicals on amyloid fibrils. We found that SNAPol-1 (with ε~50) outperformed the other two radicals. The MAS DNP experiments revealed signals of flexible side chains previously inaccessible at conventional room-temperature experiments. These results demonstrate the potential of MAS-DNP NMR as a valuable tool for structural investigations of amyloid fibrils, particularly for side chains and dynamically disordered segments otherwise hidden at room temperature.

Introduction

Amyloid fibrils are self-assembled protein aggregates that have been associated with numerous human disorders, including Alzheimer's and Parkinson's diseases.[1,2] On the other hand, some amyloid fibrils play important roles in certain physiological functions (i.e. functional amyloids).[3] For instance, functional amyloids play essential roles in hormone storage,[4] bacterial curli formations[5], or in regulated cell death mechanisms in fungi.[5,6] Their 3D structure is crucial for elucidating the structure-function relationship of these systems at the molecular level. For example, the triangular beta-solenoid amyloid fold uncovered by solid-state NMR (ssNMR) in the fungal amyloid fibrils of HET-s[7] and HELLF[8] was demonstrated to be essential for amyloid cross-seeding and required to trigger a regulated cell death reaction in filamentous fungi.[8] Due to their insolubility and lack of a crystalline order, amyloid fibrils still constitute very challenging targets for structural biology. Additionally, they often exhibit a remarkable degree of local structural polymorphism.[9] High-resolution 3D structures of amyloid fibrils can be experimentally accessed by cryo-electron microscopy (cryo-EM)[10] and magic-angle spinning (MAS) NMR.[11–14] In contrast to cryo-EM, ssNMR techniques provide access to atomic-level information on dynamics at different times scales and site-specific polymorphism.[15] However, one of the main disadvantages of ssNMR is its inherently low sensitivity, often leading to long measurement times to perform multidimensional experiments required for extracting distance restraints required for structure determination.[16] The sensitivity issue can be circumvented by employing dynamic nuclear polarization (DNP),[17,18] which is an NMR hyperpolarization technique that mediates polarization transfer from unpaired electrons or radicals to nuclei via strategic microwave irradiation. In MAS DNP experiments, gyrotrons, high-frequency microwave sources capable of generating 20-100 W of microwaves, are employed to irradiate samples at low temperatures (≤ 100 K) for efficient performances.[19–23] To cryoprotect the precious biological NMR samples, glycerol- or trehalose-water mixtures are often used to homogeneously disperse the doped radicals across the amorphous sample.[24] This hyperpolarization technique has paved the way for ssNMR to obtain important structural information on biosolids (including amyloid fibrils)[25,26,35,36,27–34] and inorganic materials that were previously inaccessible due to poor sensitivity.[37]

Although the theoretical maximum DNP enhancement factor ε is ~658 for ^{1}H nuclei, an actual experimental gain of up to 200~300 were reported in actual MAS DNP experiments performed at ~ 9 T and ≥ 80 K at 14.1 T.[38–42] The development of higher-field DNP

instruments at 18.8 T and 21.1 T is motivated by the fact that high-field NMR spectroscopy offers a better chemical-shift dispersion,[43–45] i.e., it allows NMR peaks to be better resolved and constitutes a crucial aspect for biological NMR applications. However, it is known that the main MAS-DNP mechanism, cross effect, has decreasing DNP performance (or lower ε) with increasing magnetic field.[38,46] Although pulsed DNP techniques with field-independent performances have been suggested to circumvent this issue,[47–50] their stringent microwave power requirement has limited experimental demonstrations to low fields (≤1.2 T). An alternate strategy is to design a new class of DNP polarizing agents (or hetero-biradicals) that maximally exploit the cross-effect matching conditions at high magnetic fields.[38,43,51–53] Among these novel biradicals, we will characterize the DNP performances of NATriPol-3 and SNAPol-1 radicals, which were demonstrated to yield efficient DNP performances (*vide infra*).[54,55]

Molecular motions present in biological macromolecules average NMR interactions (such as chemical shifts) over different conformations and thus may lead to narrow lines. When such motions become frozen at low temperatures required for DNP experiments, the distribution of conformational states leads to significant inhomogeneous NMR line broadening or lower peak resolution.[56] It has been reported in the literature that the line widths of some rigid biological molecules are minimally affected by the low temperatures,[57–59] and, therefore, performing experiments at cryogenic temperatures can even be advantageous. For instance, semi-rigid side chains of amino acids and mobile loop regions are challenging to observe using cross-polarization (CP) techniques at room temperature, where intermediate dynamics are too fast for dipolar-based CP transfer but too slow for *J*-based Insensitive Nuclei Exchanged by Polarization Transfer (INEPT) techniques to be applied,[60–63] resulting in weak NMR peaks that could be below the detection limit.[64–67] By observing these semi-rigid loops and side chains, a more accurate determination of their properties could be obtained from MAS DNP measurements. For instance, it will be advantageous to extract additional distance restraints from residues that are mobile and hidden at room temperature—but become more rigid at lower temperatures—for structure calculations.[68] Lowering the temperatures to observe NMR peaks of these functionally important semi-rigid parts to slow down the deleterious intermediate dynamics coincidently improves DNP performances.

In this communication, we have performed MAS DNP experiments at a high magnetic field 18.8 T (800 MHz ^{1}H Larmor frequency) using efficient hetero-biradical,

SNAPol-1, to demonstrate unprecedented ^{13}C signal enhancement ε of ~50 for amyloid fibrils. These protein assemblies exhibit a good spectral resolution in ^{13}C and ^{15}N dimensions at cryogenic temperature, enabling the observation of highly sensitive 2D ^{15}N-^{13}C correlation experiments using the PAIN-CP transfer scheme. Our results pave the way to develop DNP-enhanced ssNMR approaches using ^{15}N-^{13}C correlation experiments to reveal semi-rigid side chain signals that are otherwise hidden at room temperature. In addition, the experiments reveal new peaks that allow the extraction of structural information on less rigid protein segments in protein assemblies.

Results and Discussion

We prepared a ^{13}C, ^{15}N-labeled HET-s(218-289) protein sample, aggregated into amyloid fibrils with 5 mM M-TinyPol radical in DNP juice, which is a mixture of d_8-glycerol/D_2O/H_2O in a 6:3:1 by volume ratio. A DNP experiment was performed at 10 kHz MAS using a 3.2 mm sapphire rotor, temperature T ~100 K, and a magnetic field B_0 = 18.8 T (see SI for further experimental details). The ^{1}H-^{13}C CP spectrum showed an enhancement ε~10 (**Fig. 1b**). We have doped the same fibrillar sample with NATriPol-3 radical, which exhibited a similar performance (ε ~ 10). Note that Bahri *et al.* have recently reported a DNP study on amyloid fibrils of $A\beta_{1\text{-}42}$ using the same radical (M-TinyPol) at the same magnetic field but with a faster spinning frequency of 40 kHz using a 1.3 mm rotor,[58] which yielded to a higher ε~22, likely due to more efficient microwave penetration through the smaller rotor.[52] **Figure 1a** shows a 2D ^{13}C DARR spectrum of DNP-enhanced HET-s amyloid fibrils. We observed ^{13}C linewidths for isolated peaks in the range of ~200-300 Hz. Note that the low-

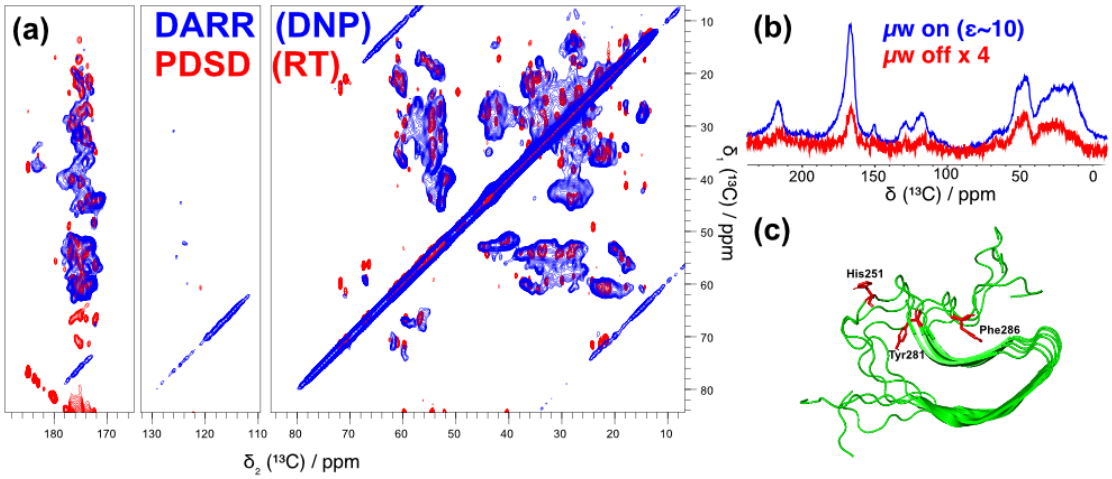

Fig. 1 (**a**) 2D ^{13}C-^{13}C 20 ms DARR spectrum of HET-s(218-289) amyloid fibrils recorded with DNP at 100 K (blue), overlayed with a 50 ms PDSD spectrum acquired at room temperature (red)**.** (**b**) 1D ^{1}H-^{13}C CP spectra of HET-s(218-289) doped with M-TinyPol under the microwave on (blue) or off (red) condition. An enhancement factor of ε~10 was observed. (**c**) 3D structure of HET-s(218-289) amyloid fibrils (PDB entry 2rnm), with aromatic residues showed with a stick representation and colored in red.

temperature DNP spectrum has 2-3x broadened lines relative to the room-temperature spectrum (overlayed in **Fig. 1a**), which has reported linewidths for the same protein system of ~100 Hz.[69] The relatively moderate line broadening effect indicates a high structural homogeneity (or rigidity) of HET-s amyloid fibrils even at a temperature of 100 K. So far, the most narrow ^{13}C linewidths at cryogenic temperatures have been reported for the $A\beta_{40}$ and $A\beta_{42}$ amyloids,[31,58] implying that both of these proteins retain a high structural homogeneity at low temperature. It is important to note that NMR linewidths in proteins under MAS depend on multiple factors, i.e., magnetic field strength, MAS frequency, processing parameters, radical concentration, and site-specific hydration.[56,68,70] To document these observations and compare our NMR data obtained on HET-s amyloid fibrils doped with NATriPol-3, we have compiled detailed ^{13}C linewidths of previously reported amyloid fibrils at low temperatures in **Table 1**. We note that the linewidths obtained in our experiments on HET-s are comparable to or even better than previously reported results in the literature.

Sample	^{13}C linewidth	B_0 field (MHz)	Apodization	T (K)	References	Remarks
HETs(218-289)	0.96-1.5 ppm 192-305 Hz	800	Qsine 3	100	This study	Extracted from 8 isolated peaks
HETs(218-289)	1-2.5 ppm 150-375 Hz	600	Qsine 2.2	100	Bauer, JBioNMR, 2017	Low temperature only (no DNP), residue-dependent
PI3 K-SH3 fibrils	2-3 ppm 200-300 Hz	400	N.A.	100	Bayro, JACS, 2011	
AB_{1-40}	0.7-0.8 ppm 140-160 Hz	850	N.A.	100	Del Amo, JBioNMR, 2013	Low temperature only (no DNP)
AB_{1-40}, protofibrils	3.0− 5.2 ppm 300-520 Hz	400	150 Hz Gaussian	25	Potapov, JACS, 2015	
AB_{1-40}, neutral pH	4.4−7.4 ppm 440-740 Hz	400	150 Hz Gaussian	25	Potapov, JACS, 2015	
AB_{1-40}, fibrils	2.4−3.2 ppm 240-320 Hz	400	150 Hz Gaussian	25	Potapov, JACS, 2015	
CsgA amyloid fibrils	2.7-4.3 ppm 270-430 Hz	400	N.A.	110	Nagaraj, ChemBioChem, 2016	Depends on the concentration of TOTAPOL radicals
AB_{1-42}	~0.6 ppm 120 Hz	800	QSine3	110	Bahri, PNAS 2022	

Table 1 Line widths of different amyloid fibrils obtained at low temperatures reported in the literature. Data that is not available is denoted by N.A.

HET-s in its fibrillar amyloid state forms a rigid β-solenoid spanning residues 226-246 (first repeat) and residues 262-282 (second repeat).[71] In the DNP experiment, we observed additional ^{13}C-^{13}C correlations involving aromatic atoms (120-130 ppm spectral region in **Fig. 1a**) that were previously absent in the experiment recorded at room temperature.

To complement the observation of ^{13}C sites, we used multidimensional ^{15}N-^{13}C spectroscopy to access ^{15}N dimension. We have observed several cross peaks in the δ (^{13}C)

~140 ppm and δ (^{15}N) ~130 ppm region in **Fig. 2** that corresponds to His residues. These His cross peaks could either be assigned to the 6-His residues from the His-tag at C-terminus of the sample, or His242 that is in the flexible loop region that connect the two beta-solenoid repeats. None of these His residues were previously observable at RT experiment. Thus, we have established an experimental set up that could allow the detection of the His residues that are otherwise not detectable at room temperature. Further experiments (i.e., a 3D NCC correlation experiment) would be required to perform an unambiguous sequential assignment of these residues.

Notably, the ^{13}C linewidths for aromatic residues have broadened marginally from ~120 Hz to ~150 Hz between the room-temperature and low-temperature DNP experiments. This implies a relatively high structural homogeneity for otherwise mobile sidechains. The 2D NCa spectrum (**Fig. 2**) exhibited quite broad ^{15}N linewidths (~300 Hz), indicating that the ^{15}N nuclei could be more sensitive to structural inhomogeneity due to cryogenic temperatures. A similar feature has also been observed for microcrystalline proteins at low temperatures.[59,68]

Interestingly, the ^{15}N-^{13}C correlation DNP spectrum revealed new peaks at ^{15}N chemical shift below 100 ppm and ^{13}C chemical shift at ~ 107 and ~ 157 ppm (labelled in **Fig. 2**), which we assigned as ^{15}N side chain nuclei. By inspecting the reported Cα chemical shifts for the HET-s(218-289) protein at RT,[71] we have assigned these correlations and we established new N-C proximities, i.e., 236ArgNζ-Cδ, 274ArgNζ-Cδ, and 270LysNζ-Cε in

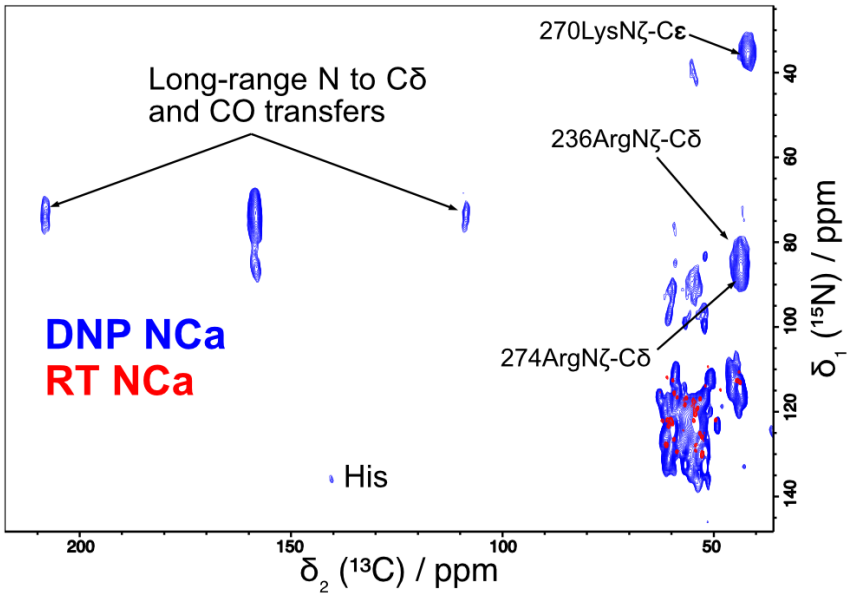

Fig. 2 2D ^{15}N-^{13}C NCa spectrum of HET-s(218-289) amyloid fibrils recorded with DNP at 100 K (red), overlayed with spectrum recorded at room temperature (blue).

the DNP spectrum (**Fig. 2**) that are helpful for sidechain assignment.

Next, we examined the DNP performance of using SNAPol-1, a trityl-nitroxide hetero-biradical that has recently demonstrated an ε ~110 on ubiquitin using a 3.2 mm DNP system at 18.8 T.[72] We added 5 mM SNAPol-1 to ^{13}C, ^{15}N-labeled NWD2 amyloid fibrils, which share a similar beta-solenoid fold as observed in HET-s,[73] and found that the SNAPol-1 sample yields a higher ^{1}H enhancement (**Fig. S1**, ε~30) than the M-TinyPol sample (ε~10). Following that, we obtained a highly promising enhancement of ε ~50 in a ^{1}H-^{13}C CP spectrum using SNAPol-1 at 11 kHz MAS frequency (**Fig. 3a**). Hence, we conclude that SNAPol-1 is a more efficient polarizing agent for DNP experiments on amyloid fibrils. Note that an additional 10 % improvement in DNP performance was achieved by performing a freeze-pump-thaw procedure, which is a known procedure that removes dissolved paramagnetic oxygen that compromises the DNP samples (see Sample Preparation).[74,75] To the best of our knowledge, ε ~50 is the highest DNP enhancement factor achieved for amyloid fibrils at 18.8 T reported to date. We anticipate that even more efficient DNP performance could be obtained for a 1.3 mm rotor due to better microwave penetration. Besides, the use of a smaller rotor could lead to fewer spinning sidebands, less spectral overlap, and narrower linewidths by spinning 4x faster (~40 kHz MAS). We also noted different enhancement factors were obtained between the simple ^{1}H direct pulse (ε ~ 30) and the CP experiment (ε ~50). This is likely a feature that depends on the accessibility of the target molecules to the solvent, and, hence, is sample dependent.[36]

The excellent signal enhancement allowed us to observe new peaks in the DNP-NCa spectrum (**Fig. 3b**). Based on their chemical shifts, these new peaks could originate from the side chains. These peaks were not observed in conventional room-temperature ssNMR experiments, probably due to unfavorable dynamics that interfere with the timescale of CP-based experiments. Hence, when frozen at low temperatures, the side chains are sufficiently rigid to allow efficient polarization transfer through dipolar couplings—they become observable in CP-based ssNMR experiments.

To ease the assignment process of these newly observed peaks and obtain new distance restraints, we set up a 2D ^{15}N-^{13}C PAIN-CP experiment,[76,77] which has been demonstrated to be efficient for obtaining the long-range heteronuclear distance restraints necessary for structure determination.[29,71,78,79] Nevertheless, it is known that setting up PAR/PAIN-CP experiments is challenging due to the sensitive matching conditions, i.e., the radiofrequency (rf) nutation frequencies applied on the ^{1}H and ^{13}C for PAR (and additionally on the ^{15}N for PAIN-CP) have to be precisely configured for optimum performances.[76,80,81]

Hence, it is common to first optimize the PAR/PAIN-CP conditions on $^{13}C/^{15}N$-labeled small peptides or model proteins before repeating the experiments on the larger and less sensitive target biomolecules. Such an optimization strategy is not ideal because the experimental parameters might be significantly different in non-crystalline proteins such as hydrated

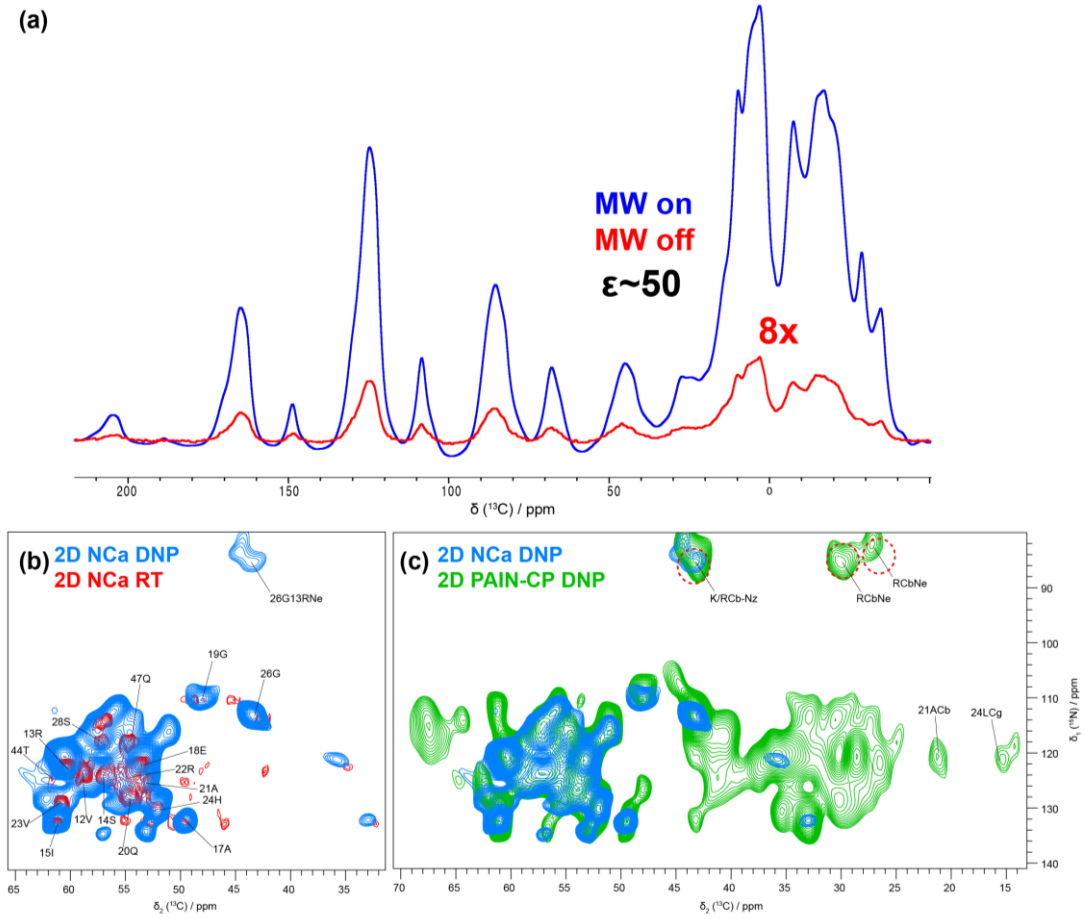

Fig. 3 (**a**) Comparison of 1D ^{1}H-^{13}C CP spectra of NWD2 amyloid fibrils with 5 mM SNAPol-1 recorded at 11 kHz MAS with microwave on (blue) and off (red) condition. Enhancement factor of ε~50 was measured. **(b)** 2D NCa spectrum recorded with DNP at 100 K and 10 kHz MAS (blue), overlayed with a similar experiment acquired at 273 K and 11 kHz MAS (red). Both spectra were recorded at 18.8 T. (**c**) DNP-enhanced ^{15}N-^{13}C PAIN-CP (green) show long-range cross peaks that are absent in DNP NCa experiments (blue).

protein assemblies, where the sample heterogeneity, rf inhomogeneity, and larger chemical shift dispersion might impede the PAR/PAIN transfer efficiency.

While it is possible to optimize the PAR/PAIN-CP condition directly on the interested proteins with a 1D spectrum, it is difficult to assess the efficiency of long-range transfers that is usually weaker and difficult to observe under the presence of stronger but less important short-range contacts. Hence, it is easier to find a robust matching condition with a 2D

experiment, despite being more time-consuming. However, thanks to the sensitivity enhancement of ε~50 bestowed by DNP, we can acquire a ^{15}N-^{13}C PAIN-CP spectrum (**Fig. 3c**) with a modest signal-to-noise ratio in only two hours. Note that an experimental time of ~208 days without DNP enhancement would have been required to record a spectrum with a similar signal-to-noise ratio. To our knowledge, a DNP-enhanced PAIN spectrum has not been demonstrated in the literature. This could be because the relatively low biradical concentration (5 mM) used here, compared to the ≥ 10 mM biradical concentration employed in the literature,[82,83] leads to longer spin-locked relaxation times, $T_{1\rho}$, and hence more efficient PAR/PAIN-CP transfer.[84] The resulting 2D ^{15}N-^{13}C PAIN-CP spectrum (**Fig. 3c**) shows numerous intra-residue correlations between backbone ^{15}N nuclei and the side chain ^{13}C nuclei. These signals are crucial to establish the amino acid spin system identification and correlating the signals observed in 2D ^{13}C-^{13}C experiments to those observed in the conventional 2D NCa experiment. In addition to ^{15}N backbone correlations, the frozen temperature conditions under DNP boost ^{15}N signals arising from side chain nitrogen, typically from Nε of Arginine and/or Nζ from lysine (ambiguous assignments for these side chains are shown in **Fig. 3c**). These residues have long side chains that keep an important mobility at room temperature, whose NMR signals can be uncovered by low-temperature DNP experiments. Note that similar correlations have also been observed for frequency-selective TEDOR experiments for bacteriorhodopsin using DNP.[85]

Experimental section

Sample preparation

The ^{13}C,^{15}N labelled HETs(218-289), and NWD2 samples were prepared according to previously published protocols.[69] Both samples were mixed with either 5 mM M-TinyPol (CortecNet) or 5 mM SNAPol-1 radicals in DNP juice (d_8-glycerol: D_2O: H_2O in a ratio of 6:3:1 by volume) and incubated for 1h at room temperature (RT). The samples were shortly centrifuged in a benchtop centrifuge (≤ 2000 g) before being packed into sapphire rotors. We have used Vespel MAS drive caps instead of the vendor-recommended ZrO_2 drive caps because the latter design has a segmented insert, which can be easily damaged if mishandled. Nevertheless, the Vespel drive caps become loose at low temperatures due to a different heat expansion coefficient from the sapphire material. Hence, we marked the inserts of the Vespel caps with a permanent marker (Sharpie) to improve the seal between the rotor and the drive cap. The DNP sample was then degassed with at least three freeze-pump-thaw cycles using a 3-way tap, and backfilled with Argon gas.[74,86] This procedure removes the paramagnetic

oxygen, which reproducibly improves the DNP enhancement factor by ~10 %. We could not implement the insert/eject cycle degassing method demonstrated in Kubicki et al. because the rotor is likely to be blocked in our Bruker MAS DNP probe at lower temperatures.[75]

MAS DNP NMR spectroscopy

The spectra were acquired on a Bruker 800 MHz spectrometer, with a wide-bore 18.8 T magnet equipped with a 3.2 mm HCN DNP probe at the temperature T = 100 K and at 8-10 kHz MAS frequencies. Note that the M-TinyPol and SNAPol-1 samples coincidentally yield the maximum positive cross-effect DNP performances at the same static magnetic field B_0 field for a fixed gyrotron microwave frequency. Hence, all DNP experiments were at B_0 = 18.796 T (^{1}H Larmor frequency of 800.28 MHz) with a gyrotron microwave frequency of 526.965 ± 0.01 GHz. The gyrotron output power of 15 W (with 130 mA collector current in the gyrotron) was used in all DNP experiments. Although the commercial probe is rated for operation at ~10-12 kHz at ~100 K, we have performed most DNP experiments at 8 kHz MAS frequency, which is significantly less likely to have rotor crash events than the experiments at 10 kHz. The spectra were processed with TopSpin 3.1 and analyzed with the CcpNmr 2.1 program.[87]

Conclusions

In summary, we have demonstrated the potential of DNP-MAS NMR in studying amyloid fibrils, particularly the semi-rigid protein segments and mobile side chains that are otherwise inaccessible in conventional room-temperature ssNMR experiments. We have obtained an enhancement factor of ε ~ 50 using SNAPol-1, which is the highest enhancement reported so far at 18.8 T for amyloid fibrils. Contrary to DNP studies reported on biomolecules, the ^{13}C nuclei in HET-s(218-289) fibrils retain a modest NMR resolution at cryogenic temperatures (T ~ 100 K) in DNP experiments. The boost of sensitivity and the low-temperature environment helps elucidate new peaks usually unobservable at room temperature due to mobility in an unfavorable regime. Additionally, we demonstrated that a 2D ^{15}N-^{13}C PAIN-CP spectrum with excellent sensitivity could be obtained in less than 2 hours. This approach allowed us to observe new correlations involving ^{15}N side chain nuclei. The promising DNP experiments and results will be combined with selective labelling schemes to obtain unambiguous distance restraints of previously unassigned peaks in the future. This will be

crucial for refining the 3D structures of biological macromolecules and gaining insights into important biological functions.

Acknowledgement

A. Loquet acknowledges financial support from the European Research Council (ERC) under the European Unions Horizon 2020 research and innovation program (ERC-2015-StG GA no. 639020). A. Lends was supported by the Swiss National Science Foundation for the early postdoc mobility project (P2EZP2_184258). K.O.T is grateful for the fundings granted by the French National Research Agency: *PulsedDNP* (ANR-20-ERC9-0008) and *HFPulsedDNP* (ANR-21-CE29-0019). Financial support from the IR INFRANALYTICS FR2054 for conducting the research is gratefully acknowledged. Y.P.L. acknowledges the support from the National Natural Science Foundation of China (Nos. 22174099 and 21871210) and Science & Technology Projects of Tianjin (No. 20JCZDJC00050).

Declarations

The authors declare that they have no conflict of interest.

Contributions

A. Lends, A. Loquet, and KOT designed the research. The NMR samples were prepared in Bordeaux, while the DNP experiments were performed at ENS. XC and YPL provided the radicals. A. Lends wrote the first draft of the manuscript. All authors prepared the figures, edited, and reviewed the manuscript.

References

1. Ke, P. C. *et al.* Half a century of amyloids: Past, present and future. *Chem. Soc. Rev.* **49**, 5473–5509 (2020).
2. Dobson, C. M., Knowles, T. P. J. & Vendruscolo, M. The amyloid phenomenon and its significance in biology and medicine. *Cold Spring Harb. Perspect. Biol.* **12**, (2020).
3. Loquet, A., Saupe, S. J. & Romero, D. Functional Amyloids in Health and Disease. *J. Mol. Biol.* **430**, 3629–3630 (2018).
4. Maji, S. K. *et al.* Functional Amyloids as Natural Storage of Peptide Hormones in Pituitary Secretory Granules. *Science (80-.).* **325**, 328–332 (2009).
5. Chapman, M. R. *et al.* Role of Escherichia coli curli operons in directing amyloid fiber

formation. *Science (80-.).* **295**, 851–855 (2002).

6. Loquet, A. & Saupe, S. J. Diversity of amyloid motifs in NLR signaling in fungi. *Biomolecules* **7**, 1–10 (2017).
7. Wasmer, C. *et al.* Amyloid fibrils of the HET-s(218-289) prion form a beta solenoid with a triangular hydrophobic core. *Science* **319**, 1523–6 (2008).
8. Daskalov, A. *et al.* Structural and molecular basis of cross-seeding barriers in amyloids. *Proc. Natl. Acad. Sci. U. S. A.* **118**, 1–8 (2020).
9. Tycko, R. Physical and structural basis for polymorphism in amyloid fibrils. *Protein Sci.* **23**, 1528–1539 (2014).
10. Fitzpatrick, A. W. & Saibil, H. R. Cryo-EM of amyloid fibrils and cellular aggregates. *Curr. Opin. Struct. Biol.* **58**, 34–42 (2019).
11. Daskalov, A. *et al.* Structures of Pathological and Functional Amyloids and Prions, a Solid-State NMR Perspective. *Front. Mol. Neurosci.* **14**, 1–18 (2021).
12. Meier, B. H. & Böckmann, A. The structure of fibrils from 'misfolded' proteins. *Curr. Opin. Struct. Biol.* **30**, 43–49 (2015).
13. van der Wel, P. C. A. Insights into protein misfolding and aggregation enabled by solid-state NMR spectroscopy. *Solid State Nucl. Magn. Reson.* **88**, 1–14 (2017).
14. Jaroniec, C. P. Two decades of progress in structural and dynamic studies of amyloids by solid-state NMR. *J. Magn. Reson.* **306**, 42–47 (2019).
15. Siemer, A. B. Advances in studying protein disorder with solid-state NMR. *Solid State Nucl. Magn. Reson.* **106**, 101643 (2020).
16. Loquet, A. *et al.* 3D structure determination of amyloid fibrils using solid-state NMR spectroscopy. *Methods* (2018). doi:10.1016/j.ymeth.2018.03.014
17. Su, Y., Andreas, L. & Griffin, R. G. Magic angle spinning NMR of proteins: high-frequency dynamic nuclear polarization and (1)H detection. *Annu. Rev. Biochem.* **84**, 465–97 (2015).
18. Nmr, B. S., Biedenb, T., Aladin, V. & Saeidpour, S. Dynamic Nuclear Polarization for Sensitivity Enhancement in. (2021). doi:10.1021/acs.chemrev.1c00776
19. Matsuki, Y., Idehara, T., Fukazawa, J. & Fujiwara, T. Advanced instrumentation for DNP-enhanced MAS NMR for higher magnetic fields and lower temperatures. *J. Magn. Reson.* **264**, 107–115 (2016).
20. Thurber, K. R., Yau, W. M. & Tycko, R. Low-temperature dynamic nuclear polarization at 9.4 T with a 30 mW microwave source. *J. Magn. Reson.* **204**, 303–313 (2010).

21. Li, Y. *et al.* Solid-state MAS NMR at ultra low temperature of hydrated alanine doped with DNP radicals. *J. Magn. Reson.* **333**, 107090 (2021).
22. Thurber, K. & Tycko, R. Low-temperature dynamic nuclear polarization with helium-cooled samples and nitrogen-driven magic-angle spinning. *J. Magn. Reson.* **264**, 99–106 (2016).
23. Sesti, E. L. *et al.* Magic angle spinning NMR below 6 K with a computational fluid dynamics analysis of fluid flow and temperature gradients. *J. Magn. Reson.* **286**, 1–9 (2018).
24. Takahashi, H., Hediger, S. & De Paëpe, G. Matrix-free dynamic nuclear polarization enables solid-state NMR 13C-13C correlation spectroscopy of proteins at natural isotopic abundance. *Chem. Commun.* **49**, 9479–9481 (2013).
25. Jaudzems, K., Polenova, T., Pintacuda, G., Oschkinat, H. & Lesage, A. DNP NMR of biomolecular assemblies. *J. Struct. Biol.* **206**, 90–98 (2019).
26. Zhao, W., Fernando, L. D., Kirui, A., Deligey, F. & Wang, T. Solid-state NMR of plant and fungal cell walls: A critical review. *Solid State Nucl. Magn. Reson.* **107**, 101660 (2020).
27. Gauto, D., Dakhlaoui, O., Marin-Montesinos, I., Hediger, S. & De Paëpe, G. Targeted DNP for biomolecular solid-state NMR. *Chem. Sci.* **12**, 6223–6237 (2021).
28. Bayro, M. J. *et al.* Intermolecular structure determination of amyloid fibrils with magic-angle spinning and dynamic nuclear polarization NMR. *J. Am. Chem. Soc.* **133**, 13967–74 (2011).
29. Debelouchina, G. T. *et al.* Higher order amyloid fibril structure by MAS NMR and DNP spectroscopy. *J. Am. Chem. Soc.* **135**, 19237–47 (2013).
30. Frederick, K. K. *et al.* Combining DNP NMR with segmental and specific labeling to study a yeast prion protein strain that is not parallel in-register. *Proc. Natl. Acad. Sci. U. S. A.* **114**, 3642–3647 (2017).
31. Lopez del Amo, J.-M., Schneider, D., Loquet, A., Lange, A. & Reif, B. Cryogenic solid state NMR studies of fibrils of the Alzheimer's disease amyloid-β peptide: perspectives for DNP. *J. Biomol. NMR* **56**, 359–363 (2013).
32. Nagaraj, M. *et al.* Surface Binding of TOTAPOL Assists Structural Investigations of Amyloid Fibrils by Dynamic Nuclear Polarization NMR Spectroscopy. *ChemBioChem* 1308–1311 (2016). doi:10.1002/cbic.201600185
33. Potapov, A., Yau, W. M., Ghirlando, R., Thurber, K. R. & Tycko, R. Successive Stages of Amyloid-β Self-Assembly Characterized by Solid-State Nuclear Magnetic

Resonance with Dynamic Nuclear Polarization. *J. Am. Chem. Soc.* **137**, 8294–8307 (2015).

34. Deo, T., Cheng, Q., Paul, S., Qiang, W. & Potapov, A. Application of DNP-enhanced solid-state NMR to studies of amyloid-β peptide interaction with lipid membranes. *Chem. Phys. Lipids* **236**, 105071 (2021).
35. Maciejko, J. *et al.* Visualizing Specific Cross-Protomer Interactions in the Homo-Oligomeric Membrane Protein Proteorhodopsin by Dynamic-Nuclear-Polarization-Enhanced Solid-State NMR. *J. Am. Chem. Soc.* **137**, 9032–9043 (2015).
36. Marin-Montesinos, I. *et al.* Selective high-resolution DNP-enhanced NMR of biomolecular binding sites. *Chem. Sci.* **10**, 3366–3374 (2019).
37. Rankin, A., Trébosc, J., Pourpoint, F., Amoureux, J.-P. & Lafon, O. Recent developments in MAS DNP-NMR of materials. *Solid State Nucl. Magn. Reson.* (2019). doi:10.1016/J.SSNMR.2019.05.009
38. Mathies, G. *et al.* Efficient Dynamic Nuclear Polarization at 800 MHz/527 GHz with Trityl-Nitroxide Biradicals. *Angew. Chemie - Int. Ed.* **54**, 11770–11774 (2015).
39. Lilly Thankamony, A. S., Wittmann, J. J., Kaushik, M. & Corzilius, B. Dynamic nuclear polarization for sensitivity enhancement in modern solid-state NMR. *Prog. Nucl. Magn. Reson. Spectrosc.* **102**–**103**, 120–195 (2017).
40. Conroy, D. W. *et al.* Probing Watson-Crick and Hoogsteen base pairing in duplex DNA using dynamic nuclear polarization solid-state NMR spectroscopy. *Proc. Natl. Acad. Sci. U. S. A.* in press (2022). doi:10.1073/pnas.2200681119/-/DCSupplemental.Published
41. Akbey, Ü., Linden, A. H. & Oschkinat, H. High-Temperature Dynamic Nuclear Polarization Enhanced Magic-Angle-Spinning NMR. *Appl. Magn. Reson.* **43**, 81–90 (2012).
42. Menzildjian, G. *et al.* Efficient Dynamic Nuclear Polarization up to 230 K with Hybrid BDPA-Nitroxide Radicals at a High Magnetic Field. *J. Phys. Chem. B* **125**, 13329–13338 (2021).
43. Lund, A. *et al.* TinyPols: a Family of Water-Soluble Binitroxides Tailored for Dynamic Nuclear Polarization Enhanced NMR Spectroscopy at 18.8 and 21.1 T. *Chem. Sci.* **68**, 42–61 (2020).
44. Felch, K. *et al.* First tests of a 527 GHz gyrotron for dynamic nuclear polarization. in *2013 IEEE 14th International Vacuum Electronics Conference (IVEC)* 1–2 (IEEE, 2013). doi:10.1109/IVEC.2013.6571048

45. Blank, M., Borchard, P., Cauffman, S., Felch, K. & Rosay, M. Development of high-frequency cw gyrotrons for DNP / NMR applications. *Terahertz Sci. Technol.* **9**, 177–186 (2016).
46. Tan, K. O., Jawla, S., Temkin, R. J. & Griffin, R. G. Pulsed Dynamic Nuclear Polarization. in *eMagRes* 339–352 (2019). doi:10.1002/9780470034590.emrstm1551
47. Henstra, A., Dirksen, P., Schmidt, J. & Wenckebach, W. T. Nuclear spin orientation via electron spin locking (NOVEL). *J. Magn. Reson.* **77**, 389–393 (1988).
48. Tan, K. O., Yang, C., Weber, R. T., Mathies, G. & Griffin, R. G. Time-optimized pulsed dynamic nuclear polarization. *Sci. Adv.* **5**, eaav6909 (2019).
49. Wili, N. *et al.* Designing broadband pulsed dynamic nuclear polarization sequences in static solids. *Sci. Adv.* **8**, 1–13 (2022).
50. Redrouthu, V. S. & Mathies, G. Efficient Pulsed Dynamic Nuclear Polarization with the X-Inverse-X Sequence. *J. Am. Chem. Soc.* **144**, 1513–1516 (2022).
51. Wisser, D. *et al.* BDPA-Nitroxide Biradicals Tailored for Efficient Dynamic Nuclear Polarization Enhanced Solid-State NMR at Magnetic Fields up to 21.1 T. *J. Am. Chem. Soc.* **140**, 13340–13349 (2018).
52. Berruyer, P. *et al.* Dynamic Nuclear Polarization Enhancement of 200 at 21.15 T Enabled by 65 kHz Magic Angle Spinning. *J. Phys. Chem. Lett.* **11**, 8386–8391 (2020).
53. Halbritter, T., Harrabi, R., Paul, S., Tol, J. Van & Lee, D. *PyrroTriPol : a Semi-rigid Trityl-Nitroxide for High Field Dynamic Nuclear Polarization*. *ChemRxiv* (2022). doi:10.26434/chemrxiv-2022-b7s7m
54. Zhai, W. *et al.* Postmodification via Thiol-Click Chemistry Yields Hydrophilic Trityl-Nitroxide Biradicals for Biomolecular High-Field Dynamic Nuclear Polarization. *J. Phys. Chem. B* **124**, 9047–9060 (2020).
55. Cai, X. *et al.* Highly Efficient Trityl- Nitroxide Biradicals for Biomolecular High- Field Dynamic Nuclear Polarization. *Chem. – A Eur. J.* **27**, 12758–12762 (2021).
56. Bauer, T. *et al.* Line-Broadening in Low-Temperature Solid-State NMR Spectra of Fibrils. *J. Biomol. NMR* **0**, 51–61 (123AD).
57. Fricke, P., Demers, J. P., Becker, S. & Lange, A. Studies on the MxiH protein in T3SS needles using DNP-enhanced ssNMR spectroscopy. *ChemPhysChem* **15**, 57–60 (2014).
58. Bahri, S. *et al.* H detection and dynamic nuclear polarization – enhanced NMR of A β 1-42 fi brils. (2022). doi:10.1073/pnas.2114413119/-/DCSupplemental.Published
59. Gauto, D. F. *et al.* Aromatic Ring Dynamics, Thermal Activation, and Transient

Conformations of a 468 kDa Enzyme by Specific 1H-13C Labeling and Fast Magic-Angle Spinning NMR. *J. Am. Chem. Soc.* **141**, 11183–11195 (2019).

60. Siemer, A. B. *et al.* Observation of highly flexible residues in amyloid fibrils of the HET-s prion. *J. Am. Chem. Soc.* **128**, 13224–13228 (2006).
61. Heise, H. *et al.* Solid-State NMR Reveals Structural Differences between Fibrils of Wild-Type and Disease-Related A53T Mutant α-Synuclein. *J. Mol. Biol.* **380**, 444–450 (2008).
62. Jirasko, V. *et al.* Dimer Organization of Membrane-Associated NS5A of Hepatitis C Virus as Determined by Highly Sensitive 1H-Detected Solid-State NMR. *Angew. Chemie - Int. Ed.* **60**, 5339–5347 (2021).
63. Ni, Q. Z. *et al.* Peptide and Protein Dynamics and Low-Temperature/DNP Magic Angle Spinning NMR. *J. Phys. Chem. B* acs.jpcb.7b02066 (2017). doi:10.1021/acs.jpcb.7b02066
64. Ravotti, F. *et al.* Solid-state NMR sequential assignment of an Amyloid-β(1–42) fibril polymorph. *Biomol. NMR Assign.* **10**, 269–276 (2016).
65. Colvin, M. T. *et al.* High Resolution Structural Characterization of Aβ<inf>42</inf> Amyloid Fibrils by Magic Angle Spinning NMR. *J. Am. Chem. Soc.* **137**, 7509–7518 (2015).
66. Gath, J. *et al.* Yet another polymorph of α-synuclein: solid-state sequential assignments. *Biomol. NMR Assign.* **8**, 395–404 (2014).
67. Wiegand, T. *et al.* Solid-state NMR sequential assignments of the N-terminal domain of HpDnaB helicase. *Biomol. NMR Assign.* **10**, 13–23 (2016).
68. Jaudzems, K. *et al.* Dynamic Nuclear Polarization-Enhanced Biomolecular NMR Spectroscopy at High Magnetic Field with Fast Magic-Angle Spinning. *Angew. Chemie - Int. Ed.* 7458–7462 (2018). doi:10.1002/anie.201801016
69. Siemer, A. B., Ritter, C., Ernst, M., Riek, R. & Meier, B. H. High-resolution solid-state NMR spectroscopy of the prion protein HET-s in its amyloid conformation. *Angew. Chemie - Int. Ed.* **44**, 2441–2444 (2005).
70. Guillaume, D. *et al.* Structural Studies of Self- Assembled Subviral Particles: Combining Cell- Free Expression with 110 kHz MAS NMR Spectroscopy. *Angew. Chemie Int. Ed.* **57**, 4787–4791 (2018).
71. Van Melckebeke, H. *et al.* Atomic-resolution three-dimensional structure of HET-s(218-289) amyloid fibrils by solid-state NMR spectroscopy. *J. Am. Chem. Soc.* **132**, 13765–75 (2010).

72. Cai, X. *et al.* Highly Efficient Trityl-Nitroxide Biradicals for Biomolecular High-Field Dynamic Nuclear Polarization. *Chem. - A Eur. J.* **27**, 12758–12762 (2021).
73. Daskalov, A. *et al.* Signal Transduction by a Fungal NOD-Like Receptor Based on Propagation of a Prion Amyloid Fold. *PLoS Biol.* **13**, 1–26 (2015).
74. Delage-Laurin, L. *et al.* Overhauser Dynamic Nuclear Polarization with Selectively Deuterated BDPA Radicals. *J. Am. Chem. Soc.* **143**, 20281–20290 (2021).
75. Kubicki, D. J. *et al.* Amplifying dynamic nuclear polarization of frozen solutions by incorporating dielectric particles. *J. Am. Chem. Soc.* **136**, 15711–15718 (2014).
76. Lewandowski, J. R., De Paëpe, G. & Griffin, R. G. Proton Assisted Insensitive Nuclei Cross Polarization. *J. Am. Chem. Soc.* **129**, 728–729 (2007).
77. Paëpe, G. De *et al.* Heteronuclear proton assisted recoupling. *J. Chem. Phys.* **134**, 1–18 (2011).
78. Colvin, M. T. *et al.* Atomic Resolution Structure of Monomorphic Aβ 42 Amyloid Fibrils. *J. Am. Chem. Soc.* **138**, 9663–9674 (2016).
79. Loquet, A. *et al.* Atomic model of the type III secretion system needle. *Nature* **486**, 276–9 (2012).
80. Donovan, K. J., Jain, S. K., Silvers, R., Linse, S. & Griffin, R. G. Proton-Assisted Recoupling (PAR) in Peptides and Proteins. *J. Phys. Chem. B* **121**, 10804–10817 (2017).
81. Donovan, K. J., Silvers, R., Linse, S. & Griffin, R. G. 3D MAS NMR Experiment Utilizing Through-Space 15 N– 15 N Correlations. *J. Am. Chem. Soc.* **139**, 6518–6521 (2017).
82. Sauvée, C. *et al.* Highly efficient, water-soluble polarizing agents for dynamic nuclear polarization at high frequency. *Angew. Chemie - Int. Ed.* **52**, 10858–10861 (2013).
83. Fricke, P. *et al.* High resolution observed in 800 MHz DNP spectra of extremely rigid type III secretion needles. *J. Biomol. NMR* **65**, 121–126 (2016).
84. Corzilius, B., Andreas, L. B., Smith, A. A., Ni, Q. Z. & Griffin, R. G. Paramagnet induced signal quenching in MAS-DNP experiments in frozen homogeneous solutions. *J. Magn. Reson.* **240**, 113–23 (2014).
85. Bajaj, V. S., Mak-Jurkauskas, M. L., Belenky, M., Herzfeld, J. & Griffin, R. G. DNP enhanced frequency-selective TEDOR experiments in bacteriorhodopsin. *J. Magn. Reson.* **202**, 9–13 (2010).
86. Tan, K. O. *et al.* Observing Nearby Nuclei on Paramagnetic Trityls and MOFs via DNP and Electron Decoupling. *Chem. – A Eur. J.* (2022).

doi:10.1002/chem.202202556

87. Vranken, W. F. *et al.* The CCPN data model for NMR spectroscopy: Development of a software pipeline. *Proteins Struct. Funct. Genet.* **59**, 687–696 (2005).